New reactions of diazene and related species for modeling combustion of amine fuels

Marshall, Paul; Rawling, George; Glarborg, Peter

Published in:
Molecular Physics

Link to article, DOI:
10.1080/00268976.2021.1979674

Publication date:
2021

Document Version
Peer reviewed version

New reactions of diazene and related species for modeling combustion of amine fuels

Paul Marshall, George R. Rawling

Department of Chemistry and Center for Advanced Scientific Computing and Modeling, University of North Texas, 1155 Union Circle #305070, Denton, Texas 76203-5017

Peter Glarborg

Department of Chemical and Biochemical Engineering, Technical University of Denmark, DK-2800 Kgs. Lyngby, Denmark

---

Potential energy surfaces for reactions involving N_2H_2 isomers of diazene (diimide) have been explored using density functional theory, with energies based on coupled-cluster theory. A focus is on processes that create or consume these species, and isomerization between the E (trans) and Z (cis) forms of HNNH. These include isomerization and dissociation pathways for HNNH, addition of H atoms to form N_2H_3, abstraction by H atoms yielding short-lived NNH, and abstraction reactions of H with N_2H_3. Transition state and capture theories are applied for high-pressure-limiting behavior, while low-pressure and falloff regions are characterized via the methods of Troe and coworkers. Rate constants and thermochemistry are provided to improve models of diamine chemistry, relevant to the combustion of NH_3 especially at high concentrations, high pressures or under reducing conditions. Results indicate that amine radical recombination mainly yields the E HNNH isomer, while H-abstraction from N_2H_3 results in E HNNH and H_2NN. However, at elevated temperature E $\rightarrow$ Z isomerization becomes competitive, and Z HNNH, being more reactive, acts to enhance the diazene consumption rate.

---

1 Introduction

The high temperature chemistry of ammonia has been of interest for several decades due to its importance for formation of nitrogen oxides (NO_x) from organically bound nitrogen in fuels [1,2], as well as for NO_x control by selective non-catalytic reduction (SNCR) using NH_3 [2]. Common for these processes is that the ammonia is present only in trace amounts and formation of N_2-amines can be neglected. Currently there is increasing interest in investigating ammonia as a potential carbon-free energy carrier [3–6]. This application is quite different from fuel-NO formation and SNCR in that it involves high concentrations of NH_3 and, for applications in engines and gas turbines, high pressure. These conditions favor formation of N_2-amines such as hydrazine (N_2H_4) and diazene (HNNH). These species are formed from recombination of amine radicals, i.e.,

$$NH_2 + NH_2(+M) \rightleftharpoons N_2H_4(+M)$$

$$NH_2 + NH \rightleftharpoons HNNH + H$$

The chemistry of diazene, formed directly by amine-amine reactions or from sequential H-abstraction from N_2H_4, has been shown to be important for predicting flame speeds of ammonia [7–9] and hydrazine [10], as well as for oxidation of NH_3 under flow reactor conditions [11]. It may also play a role in the uncatalyzed, homogeneous formation of NH_3 directly from molecular nitrogen and hydrogen [12].

While there has been a significant amount of work on dissociation of N_2H_4 and its formation from recombination of NH_2 radicals [13–15], less is known about the HNNH(+M) reaction. The detailed energetics, structures, and isomerization pathways of diazene have been investigated in numerous theoretical studies [12, 16–30]. However, results on rate constants for isomerization and dissociation of HNNH as a function of temperature and pressure are very limited. Dean and

Bozzelli [31] calculated rate constants for HNNH dissociation and isomerization to H_2NN at selected pressures, but the results were obtained at a comparatively low level of theory. More recently, Hwang and Mebel [12] estimated the high pressure limit for isomerization of H_2NN to HNNH.

A complication arises in that HNNH is energetically accessible in both trans (E HNNH or tHNNH) and cis (Z HNNH or cHNNH) configurations. Most attention has been paid to the most stable isomer, the E (trans) structure. Given the substantial barrier to E-Z isomerization in HNNH, it is not clear under what conditions the two isomers should be treated as distinct species with unique reactivities, or when rapid equilibration can be expected. We apply quantum chemistry methods and unimolecular rate theory to characterize the pressure and temperature dependence of E-Z conversion, and also to compare some production and consumption pathways for these two isomers and the higher energy H_2NN isomer in the context of N/H chemistry.

2 Theoretical approach

The potential energy surface for HNNH and its unimolecular decomposition was initially explored with density functional theory. Geometries and vibrational frequencies for minima and saddle points (transition states, TSs) were obtained with the M06-2X functional [32] and the 6-311++G(2df,2p) basis set [33]. TSs were verified by following the reaction coordinate. The M06-2X frequencies were scaled [34] by a factor of 0.970 for zero-point vibrational energy (ZPE), and by a factor of 0.944 to approximate fundamental frequencies. Next, single-point energies were obtained via the CBS-APNO method which through coupled-cluster and other calculations approximately extrapolates CCSD(T) theory to the complete basis set limit [35]. These calculations were performed with the Gaussian16 program [36]. Table 1S in the Supplementary Information summarizes the raw computational data, while relative enthalpies at 0 K derived from differences

between total energies (ZPE plus CBS-APNO electronic energy) are given in Table 1. These are equivalent to energies on the vibrationally adiabatic potential. It may be seen that agreement with precisely known thermochemistry from the Active Thermochemical Tables [37] is excellent, with a root-mean-square deviation of 0.7 kJ mol^{-1}. We therefore expect reasonable accuracy for computed barrier heights too, and employ this theory for relative enthalpies. As a check, Table 1 also shows the results of a direct $1/n^3$ CBS extrapolation of CCSD(T) calculations made with the aug-cc-pVQZ and aug-cc-pV5Z basis sets, performed with Cfour [38], which yield a root-mean-square deviation of 1.0 kJ mol^{-1} from ATcT data [37]. Unless otherwise noted, all the singlet species were treated with spin-restricted theory.

Species	H_{rel} CBS-APNO	H_{rel} CCSD(T)/CBS	H_{rel} from ATcT[a]
E HNNH	0	0	0
Z HNNH	22.1	20.9	21.7
H_2NN	99.1	99.9	100.3
H + NNH	260.6	262.5	261.1
N_2 + H_2	-207.5	-206.2	-207.1

a: Active Thermochemical Tables [37]

Table 1: Comparison of relative enthalpies at 0 K (kJ mol^{-1}).

The lower-lying reaction paths are displayed in Fig. 1, including isomerization between the E (*trans*) isomer of HNNH and the Z (*cis*) isomer,

$$\text{E HNNH(+M)} \rightarrow \text{Z HNNH(+M)} \qquad \text{(R1)}$$

The reaction numbering refers to the mechanism listing in Table 4 below. E HNNH is more stable than Z HNNH, and the interconversion via in-plane HNNH bending ("inversion") has the lowest energy barrier E_0 at TS1a. Nevertheless it is substantial at over 200 kJ mol^{-1} and so the rate constant k_{1a} for isomerization via bending (R1a) will be small at low to moderate temperatures. A second isomerization path (R1b) involves twisting around the N-N bond. This torsional TS1b has multireference character because breaking the N-N π bond creates a singlet diradical, and we rely on the MRCI+Q analysis by Biczysko et al. [28].

They computed a barrier via TS1b that was 16.3 kJ mol^{-1} higher than for TS1a, and we apply that energy difference to our E_0 result for TS1a, along with their MCSCF vibrational frequencies. For TS1b, our real spin-unrestricted M06-2X/6-311++G(2df,2p) frequencies, with $<S^2> = 1.0$, are similar and we employ the corresponding imaginary frequency.

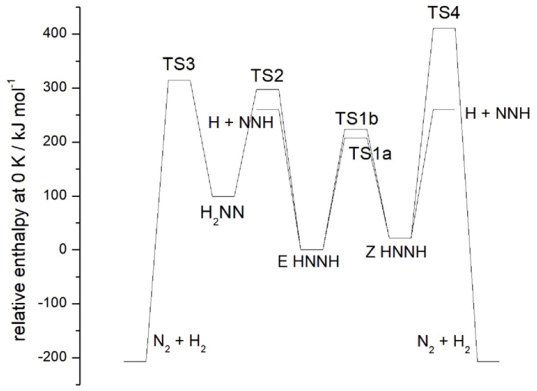

Figure 1: Relative enthalpies of low-lying paths for HNNH, computed as discussed in the text.

The pathways for dissociation of the two HNNH isomers to H + NNH appear to have no barrier beyond the endothermicity [28] and so will have loose TSs with large pre-exponential factors. Together with lower barriers, this will make the rate constant k_2 for

$$\text{E HNNH(+M)} \rightarrow \text{H} + \text{NNH(+M)} \qquad \text{(R2)}$$

significantly greater than the competing isomerization through TS2

$$\text{E HNNH(+M)} \rightarrow \text{H}_2\text{NN(+M)}$$

Accordingly we have not reanalyzed the kinetics for H_2NN formation and its

subsequent dissociation to N_2 + H_2 via TS3. Following step 2, metastable NNH has a short lifetime of around 10^{-9} s [39] with respect to dissociation via tunneling out of the ground state to make H + N_2. A similar argument leads to the conclusion that k_3 for

$$\text{Z HNNH(+M)} \rightarrow \text{H} + \text{NNH(+M)} \tag{R3}$$

will dominate over the symmetry forbidden 4-center elimination through TS4

$$\text{Z HNNH(+M)} \rightarrow \text{H}_2 + \text{N}_2\text{(+M)}$$

We note the wavefunction here exhibits RHF $\rightarrow$ UHF instability and rely on the MRCI+Q analysis by Biczysko et al. [28] for a barrier of 389 kJ mol^{-1}, which is too high for the latter reaction to be significant.

We now predict the kinetics in terms of k_1, k_2 and k_3 via unimolecular rate theory, and employ the methods developed by Troe and coworkers [40]. The Lindemann-Hinshelwood model based on collisional energy transfer between reacting molecules AB and the bath gas M

$$\text{AB} + \text{M} \rightleftarrows \text{AB} * + \text{M} \rightarrow \text{A} + \text{B} \tag{1}$$

leads to a second-order rate constant k_0 as [M] $\rightarrow$ 0 so that the effective first-order loss rate is k_0[M] at the low-pressure limit. As [M] $\rightarrow \infty$ the first-order loss rate is k_∞ at the high-pressure limit. In the intervening falloff region the general first order rate constant may be written (with F=1) as

$$\text{k} = \text{F} \times \text{k}_0[\text{M}]\text{k}_\infty/(\text{k}_\infty + \text{k}_0[\text{M}] \tag{2}$$

This generally predicts too sharp of a falloff and more realistic behavior is obtained by multiplying the above k by a broadening factor F, where F $\leq$ 1. The essence of the unimolecular methodology we apply is to use molecular properties

coupled with parameterized results from Master Equation analyses to quantify k_0, k_∞ and F. Full details have been provided by Troe and coworkers; here we give an overview of the procedure we followed.

For reaction 1 with two rigid TSs for the isomerization pathways, k_∞ was obtained via conventional transition state theory (TST), with all modes of the reactant and TS treated as harmonic oscillators and an Eckart tunneling correction. k_0 was obtained via the relation

$$k_0 = \beta_c Z_{LJ} (\rho_{vib}(E_0) RT/Q_{vib}) e^{-E_0/RT} F_{anh} F_E F_{rot\ int} \quad (3)$$

where the symbols have their usual meanings [40]. E_0 is the threshold energy for reaction. There are no hindered rotors in the species considered here, so $F_{rot\ int} = 1$. The other F terms are correction factors. F_{anh} reflects the influence of vibrational anharmonicity, F_E corrects the vibrational density of states ρ_{vib} for its energy dependence, and F_{rot} corrects for the effects of molecular rotation. Here it is controlled by the ratio of the moments of inertia in the rigid TS and the reactant, I^+/I. Z_{LJ} is the Lennard-Jones collision rate constant between reactant and bath gas, while β_c is the collisional efficiency. It is related to the average energy transferred per collision $< \Delta E >$ via

$$\beta_c/(1-\beta_c^{1/2}) = - < \Delta E > /(F_E RT) \quad (4)$$

For the bath gas $M = N_2$, we used a typical value of $-<\Delta E> = 1.9$ kJ mol^{-1} which implies $\beta_c = 0.3$ at room temperature [40]. $-<\Delta E>$ may vary slightly with temperature, either increasing or decreasing, but in the absence of detailed information we set it as a constant. Future experiments may allow a calibration of β_c and any temperature dependence. With this assumption, β_c decreases with increasing temperature and is 0.13 at 1000 K, dropping to 0.037 at 3000 K.

The center broadening factor F_{cent} refers to broadening at the center of the falloff

region [40–42], and in this work we neglect the minor impact of asymmetry in the falloff curve of k vs [M]. F_{cent} can be resolved as the product of two components

$$F_{cent} = F_{cent}^{SC} F_{cent}^{WC} \tag{5}$$

F_{cent}^{SC} refers to the strong collision assumption where $\beta_c = 1$ and single collisions with the bath gas are sufficient to energize and de-energize AB in the scheme of eq. 1, and is derived via the Kassel integral S_K. For a rigid TS with s-1 normal modes with real frequencies, we use [43]

$$S_K = 1 + \Sigma_{i=1}^{s-1} \frac{h\nu_i^{\ddagger}/k_B T}{\exp(h\nu_i^{\ddagger}/k_B T) - 1} \tag{6}$$

followed by the approximation

$$F_{cent}^{SC} = {S_K}^{-0.62} \tag{7}$$

Eq. 7 is strictly derived for room temperature and below, and the accuracy of extrapolation to elevated temperatures remains to be quantified. The contribution F_{cent}^{WC} from weak collision ($\beta_c < 1$) effects is found [42] from

$$F_{cent}^{WC} = \max\{\beta_c^{0.14}, 0.64\} \tag{8}$$

The results from eqq. 7 and 8 are combined as in eq. 5. The resulting F_{cent} parameter varies with temperature and can be expressed in the form [44]

$$F_{cent} = a \exp(-T/b) + (1 - a) \exp(-T/c) \tag{9}$$

where a, b and c are found by a least-squares fit to (T, F_{center}) data. This completes the determination of the three quantities that determine the general first-order rate constant k(T,[M]) from 800 to 3000 K. The lower temperature limit is where k_∞ becomes too small to be important relative to other processes, chosen as ca. 1 s^{-1}. The parameterizations of k_0, k_∞ and F_{cent} as functions

of temperature are provided in Table 4 below. Quantum mechanical tunneling is not incorporated in eqq. 3-9 which adds extra uncertainty to rate constants at the low end of the temperature range, especially at very low pressures. Our transition state theory analysis indicates that for N_2H_3 isomerization, tunneling enhances reactivity at the high-pressure limit by a factor of ca. 1.5 at 800 K, decreasing to 1.2 at 1300 K and less than 1.05 at 2000 K.

The remaining task is to evaluate k(T,[M]) via eq. 2. Troe's falloff formalism [40, 42] may be applied based on k_0, k_∞ and F_{cent}. The key relation is that the broadening parameter F in eq. 2 may be found via

$$\log_{10}F = \log_{10}F_{cent}/[1 + (\log(k_0[M]/k_\infty)/N)^2] \text{ with } N = 0.75 - 1.27\log_{10}F_{cent} \quad (10)$$

This procedure, eqq. 3 through 10, was modified for the E HNNH dissociation to H + NNH, because there is no barrier in the reverse direction [28], as confirmed by searches using density functional theory. First, the reverse rate constant $k_{-2,\infty}$ for H + NNH association was assessed via classical capture theory based on a $-C_6/r^6$ potential. We estimate that dipole-induced dipole interactions contribute $-2.6 \cdot 10^{-79}$ J m^6 to C_6, with a dominant contribution of $-17.7 \cdot 10^{-79}$ J m^6 from dispersion forces, which leads [45] to $k_{-2,\infty} = 2.5 \cdot 10^{14} T^{1/6}$ cm^3 mol^{-1} s^{-1}. The high-pressure limit in the forward direction $k_{2,\infty}$ was found via the association kinetics and the computed equilibrium constant.

The low-pressure limit $k_{2,0}$ was found as before via eq. 3, with one major difference. F_{rot} is now controlled by the locations of J-dependent centrifugal barriers in the long-range potential between dissociating fragments. We made the choice, with a resulting simple evaluation of F_{rot}, to assume a C_6 potential again, but note that more sophisticated approaches may be appropriate as discussed by Troe [40]. This would require more detailed information about the separating radicals which is hard to access either experimentally or computationally, and is deferred to a future study. The same collisional efficiencyβ_c is assumed as

before.

The lack of a well-defined saddle point along the reaction coordinate requires an alternative approach for the Kassel integral S_K. We used the proposal [41] that

$$E_{a,\infty} = E_0 + RT\ S_K + R\frac{\partial \ln Q}{\partial 1/T} \tag{11}$$

where $E_{a,\infty}$ is the activation energy for the high-pressure limit, readily found from an Arrhenius plot of $k_{2,\infty}$ (which is remarkably linear), E_0 is the threshold energy, and Q is the partition function for the internal modes of the reactant. The contributions to the center broadening factor were then evaluated as before.

Dissociation of Z HNNH was treated in the same way, with the same reverse association rate constant at high pressures but reversed via the different equilibrium constant appropriate for the less stable Z isomer. We found the center broadening factor to be the same, to within ca. 2%, as for E HNNH so the latter F_{cent} values were used without adjustment.

Next we investigated interactions of HNNH isomers with H atoms. Figure 2 summarizes energies obtained via the methodology outlined above, for TS5 and TS6 for the addition reactions

$$H + E\ HNNH(+M) \rightarrow N_2H_3(+M) \tag{R4}$$

$$H + Z\ HNNH(+M) \rightarrow N_2H_3(+M) \tag{R5}$$

respectively. Similar results were recently obtained by Dievart and Catoire [46] and so we did not analyze the thermal rate constants further. These pathways, in the reverse direction, are also important for the decomposition of chemically activated N_2H_3 formed from the addition of NH to NH_2 at energies, measured from v=0 for N_2H_2, of $E \geq 312.8$ kJ mol^{-1} [37]. The fundamental microcanon-

ical TST result for unimolecular decomposition is

$$k(E) = G(E - E_0^{\ddagger})/\{hN(E)\} \tag{12}$$

where G is the sum of states at the TS with energy $E - E_0^{\ddagger}$ and N is the density of states of the reactant N_2H_3 at energy E. The ratio of dissociation products, through different barriers $E_0^{\ddagger}$, will therefore be approximately the ratio of the G values. Here we neglect formation of H + H_2NN because these are much less favorable energetically, despite its occurrence through a loose transition state. We comment that a more complete analysis would incorporate angular momentum effects via k(E,J) [47].

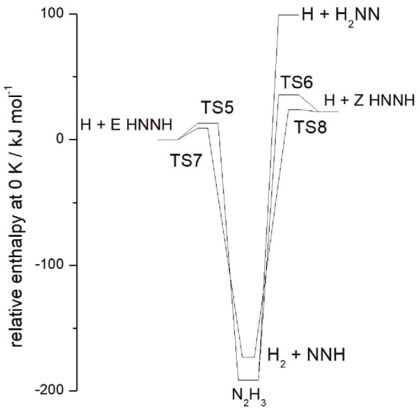

Figure 2: Relative enthalpies of low-lying paths for N_2H_3, computed as discussed in the text.

Figure 2 also shows the energetics for TS7 and TS8 which describe the abstraction pathways, respectively

$$H + E\ HNNH \rightarrow H_2 + NNH \tag{R6}$$

$$H + Z\ HNNH \rightarrow H_2 + NNH \tag{R7}$$

which we evaluated via simple TST. We also calculated the rate constant for the H-assisted isomerization via

$$\mathrm{H + Z\ HNNH \rightarrow H + E\ HNNH} \tag{R8}$$

Abstraction by atomic H of an H-atom from the different sites in N_2H_3 leads to H_2 plus H_2NN, E HNNH or Z HNNH along triplet pathways. Transition states TS9, TS10 and TS11, respectively, for each of the pathways were characterized with M06-2X/6-311++G(2df,2p) theory as outlined earlier, and then barrier heights were based on energies obtained with CCSD(T)-F12b/aug-cc-pVQZ calculations. Again, simple TST was employed to derive the rate constants.

3 Results and discussion

Cartesian coordinates of the species analyzed computationally are provided in the Supplemental Information in Table S1, along with harmonic frequencies, rotational constants and the T1 diagnostic [48]. This tests for multireference behavior which would degrade performance of the coupled-cluster-based methods we use for relative energies. We find most of the closed and open-shell species in Table S1 fall below the recommended thresholds of 0.02 and 0.044, respectively, but TS5 and TS6 for H addition to E/Z HNNH slightly exceed these limits at 0.047 and 0.048. Fortunately the extra uncertainty in energy is for minor paths, and the H + E/Z HNNH abstraction dominates as discussed below.

Table 2 lists the reactions analyzed here, and the derived enthalpy barriers or threshold energy $E_0^{\ddagger}$ and the reaction enthalpies $\Delta_r H$, both at 0 K. The parameterizations of the rate constants for reactions R1a, R1b, and R2-R7 are provided in the mechanism listing.

Reaction	$E_0^{\ddagger}$ / kJ mol^{-1}	$\Delta_r H$ / kJ mol^{-1}
E HNNH $\rightarrow$ Z HNNH TS1a	207.5	22.1
E HNNH $\rightarrow$ Z HNNH TS1b	223.8	22.1
E HNNH $\rightarrow$ H_2NN TS2	297.2	99.1
$H_2NN \rightarrow N_2 + H_2$ TS3	215.4	-306.6
E HNNH $\rightarrow$ H + NNH	260.6	260.6
Z HNNH $\rightarrow$ $N_2 + H_2$ TS4	388.9	-229.7
Z HNNH $\rightarrow$ H + NNH	238.5	238.5
$N_2H_3 \rightarrow$ H + E HNNH TS5	204.3	191.3
$N_2H_3 \rightarrow$ H + Z HNNH TS6	227.0	213.4
$N_2H_3 \rightarrow H + H_2NN$	290.4	290.4
H + E HNNH $\rightarrow$ H_2 + NNH TS7	9.0	-173.3
H + Z HNNH $\rightarrow$ H_2 + NNH TS8	1.6	-195.4
$H + H_2NN \rightarrow H_2$ + NNH	$\sim$0	-272.4
$H + N_2H_3 \rightarrow H_2$ + E HNNH	39.8	-241.6
$H + N_2H_3 \rightarrow H_2$ + Z HNNH	52.1	-220.6
$H + N_2H_3 \rightarrow H_2 + H_2NN$	10.5	-141.7

Table 2: Computed (see text) enthalpy barriers or threshold energies $E_0^{\ddagger}$ and reaction enthalpies $\Delta_r H$ for selected reactions at 0 K.

Figure 3 compares the calculated rate constants for dissociation of E HNNH and Z HNNH to NNH + H at atmospheric pressure with the value proposed by Dean and Bozzelli [31]. The dissociation of the cis isomer is calculated to be significantly faster than that of the trans isomer, with a difference of almost two orders of magnitude.

Dean and Bozzelli do not distinguish between the cis and trans isomers. However, if their dissociation rate is taken as a weighted average for the cis and trans isomers, their results are in reasonable agreement with the present findings.

We find the NH + $NH_2 \rightarrow N_2H_3^* \rightarrow$ H + HNNH process (R8, R9) to favor the E isomer by a factor of 3.2 for excitation of N_2H_3 at the threshold energy of 312.8 kJ mol^{-1}. This ratio reflects the lower barrier for dissociation to make E HNNH rather than Z HNNH, and we use it as an estimate for the overall branching ratio. For formation of H_2N_2 species from H-atom abstraction reactions with N_2H_3, the lowest barrier pathway leads to H_2NN formation, followed by E HNNH, with Z HNNH the least favorable product. Surprisingly, the strongest N-H

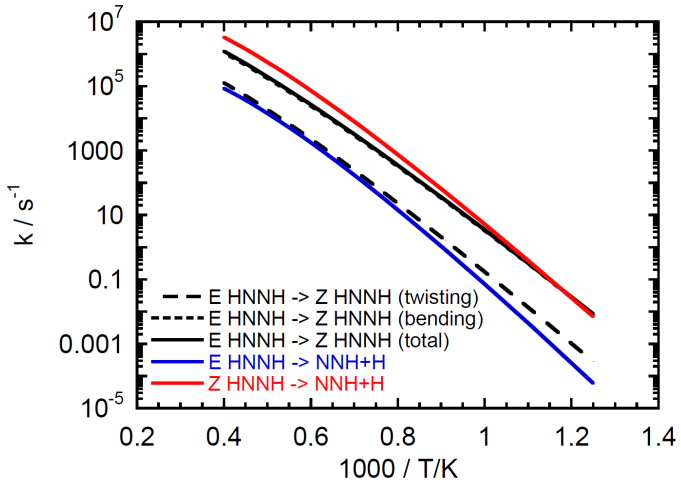

Figure 3: Arrhenius plot for isomerization and dissociation of HNNH at atmospheric pressure, based on the rate constants calculated in the present work.

bonds show the highest reactivity.

4 Implications for kinetic modeling

Formation of N_2-amines are favored at high ammonia concentrations, reducing conditions, and elevated pressure, and the N_2-amine chemistry has implications for modeling both the flame speed [7–9] and oxidation rate [11] of ammonia. In this section, the formation and consumption of HNNH in ammonia combustion are discussed, emphasizing the role of the isomers E HNNH, Z HNNH, and H_2NN. The basis for the discussion is the thermochemistry and kinetic data shown in Tables 3 and 4, respectively; to a large extent based on the present work.

Table 3 lists thermodynamic properties for N_2H_3, the N_2H_2 isomers, and NNH. The most reliable data sources are the Active Thermochemical Tables (ATcT) [49], based on a network approach, and the Burcat database [50], partly based on the ATcT data, both of which are continuously and carefully updated and

Species	H_{298}	S_{298}	$C_{p,300}$	$C_{p,400}$	$C_{p,500}$	$C_{p,600}$	$C_{p,800}$	$C_{p,1000}$	$C_{p,1500}$	Ref.
N_2H_3	225.0	236.9	42.67	49.32	55.69	61.30	69.97	76.87	88.39	[2, 49, 50]
E HNNH	200.1	218.1	35.13	38.90	43.13	47.40	55.06	60.80	70.05	pw
Z HNNH	221.8	218.3	34.92	38.48	42.59	46.81	54.39	60.21	69.59	pw
H_2NN	301.1	218.3	35.84	39.40	43.63	47.90	55.31	61.21	70.22	[2, 50]
NNH	250.0	224.6	34.42	36.09	38.14	40.24	44.05	47.15	51.75	[2, 39]

Table 3: Thermodynamic properties of selected species in the reaction mechanism. Units are kJ mol^{-1} for H, and J mol^{-1} K^{-1} for S and C_p. Temperature (T) range is in K.

documented. The thermochemistry of the N_2-amines has been in discussion. Early modeling studies of NH_3 oxidation, e.g., [39, 51, 52], used data for N_2H_3 from the Sandia Thermodynamic Database [53], implying a value for the heat of formation of 154 kJ mol^{-1}. This value is significantly lower than the recent recommendation of 225 kJ mol^{-1} from the Active Thermochemical Tables (ATcT) by Ruscic [37] and supported by a recent theoretical study [46]. This large error may have had implications for the earlier modeling studies.

In the present work, we calculated S, C_p and H_T-H_{298} for the E HNNH and Z HNNH isomers, facilitating their inclusion as separate species in kinetic models. The data, shown in Table 3, are in excellent agreement with values for HNNH and Z HNNH, respectively, from the Burcat database [50]. Trans-diazene has a heat of formation about 20 kJ mol^{-1} below that of the cis configuration. Under conditions where the cis and trans isomers are equilibrated, E HNNH is predominant, but at combustion temperatures the cis form accounts for about 20 to 30% of total diazene [46].

Earlier work on H-abstraction from HNNH has focused on the trans isomer or assumed the E and Z isomers to be equilibrated [46, 54, 55, 57–59]. However, Dievart and Catoire [46] reported that the energy barriers for cis-isomer are consistently lower than those of the trans-isomer, by 6.3, 10.5, and 19 kJ mol^{-1} for the reactions with H, CH_3, and NH_2, respectively. Consequently, formation of Z HNNH will serve to enhance the consumption rate of the diazene.

		A	β	E_a/R	Source
1a.	E HNNH(+M) $\rightleftarrows$ Z HNNH(+M)	4.9E09	1.180	24000	pw (bending)
	Low pressure limit:	3.0E28	-3.560	28200	
	Troe parameters: 0.35 650 10600				
1b.	E HNNH(+M) $\rightleftarrows$ Z HNNH(+M)	1.5E14	0.000	27700	pw (twisting)
	Low pressure limit:	2.3E29	-4.000	30250	
	Troe parameters: 0.35 650 10600				
2.	E HNNH(+M) $\rightleftarrows$ NNH + H(+M)	6.3E16	0.000	32200	pw
	Low pressure limit:	8.7E39	-6.910	35400	
	Troe parameters: 0.44 520 6150				
3.	Z HNNH(+M) $\rightleftarrows$ NNH + H(+M)	5.7E16	0.000	29500	pw
	Low pressure limit:	9.6E35	-5.440	32200	
	Troe parameters: 0.44 520 6150				
4.	N_2H_3(+M) $\rightleftarrows$ E HNNH(+M)	1.3E11	0.819	24200	[46]
	Low pressure limit:	3.8E40	-6.880	27400	
	Troe parameters: 0.168 80000 28 7298				
5.	N_2H_3(+M) $\rightleftarrows$ Z HNNH(+M)		slow		
6.	E HNNH + H $\rightleftharpoons$ NNH + H_2	9.6E07	1.800	450	pw
7.	Z HNNH + H $\rightleftharpoons$ NNH + H_2	2.8E08	1.720	240	pw
8.	Z HNNH + H $\rightleftharpoons$ E HNNH + H	7.8E08	1.580	1100	pw, low pressure limit
9.	NH_2 + NH $\rightleftharpoons$ E HNNH + H	3.3E14	-0.272	-39	[13], pw
10.	NH_2 + NH $\rightleftharpoons$ Z HNNH + H	1.0E14	-0.272	-39	[13], pw
11.	NH_2 + NH_2 $\rightleftharpoons$ HNNH + H_2	1.7E08	1.020	5930	[13]
12.	HNNH + O $\rightleftharpoons$ NNH + OH	1.1E08	1.620	405	[54]
13.	tHNNH + OH $\rightleftharpoons$ NNH + H_2O	5.9E01	3.400	684	[55]
14.	HNNH + NH_2 $\rightleftharpoons$ NNH + NH_3	2.7E05	2.226	-520	[46]
15.	N_2H_3 + H $\rightleftharpoons$ E HNNH + H_2	4.6E01	3.530	1890	pw
16.	N_2H_3 + H $\rightleftharpoons$ Z HNNH + H_2	2.7E02	3.180	3330	pw
17.	N_2H_3 + H $\rightleftharpoons$ H_2NN + H_2	3.1E06	2.110	146	pw
18.	N_2H_3 + H $\rightleftharpoons$ NH_2 + NH_2	1.0E14	0.000	0	[56], est
19.	N_2H_3 + NH_2 $\rightleftharpoons$ E HNNH + NH_3	6.1E-1	3.574	600	[46]
20.	N_2H_3 + NH_2 $\rightleftharpoons$ H_2NN + NH_3	1.1E01	3.080	106	[46]

Table 4: Selected reactions in the HNNH subset. Parameters for use in the modified Arrhenius expression $k = AT^{\beta}\exp(-E/[RT])$. Units are mol, cm, s, K. The Troe parameters correspond to eq. 9.

In order to assess the importance of distinguishing between the trans and cis isomers of diazene in modeling, let us take a look at formation and consumption pathways. Formation of HNNH in amine pyrolysis or combustion may proceed through reaction of two amine radicals,

$$NH_2 + NH \rightleftharpoons HNNH + H \qquad (R9, R10)$$

$$NH_2 + NH_2 \rightleftharpoons HNNH + H_2 \qquad (R11)$$

or by eliminating or abstracting H from N_2H_3,

$$N_2H_3(+M) \rightleftharpoons HNNH + H(+M) \qquad (R4, R5)$$

$$N_2H_3 + X \rightleftharpoons HNNH + XH$$

As discussed in section 3, the NH_2 + NH reaction yields predominantly E HNNH (R9), while formation of Z HNNH (R10) is a minor channel (less than 25%). Formation of diazene from NH_2 + NH_2 (R11) has a considerable barrier [13] and will under most conditions of interest be small compared to recombination to hydrazine,

$$NH_2 + NH_2(+M) \rightleftharpoons N_2H_4(+M)$$

Hydrazine will be consumed mainly by H-abstraction reactions [10], yielding N_2H_3. Abstraction of hydrogen from N_2H_3 yields either diazene (HNNH) or isodiazene (H_2NN).

Figure 4 shows an Arrhenius plot for the N_2H_3 + H reaction, based on the ab initio results. It is a very fast reaction, with an overall rate constant close to collision efficiency. Perhaps a bit unexpected, the H-abstraction mainly occurs on the nitrogen radical site, yielding H_2NN. Among the cis and trans isomers, formation of E HNNH dominates and Z HNNH is at most a very minor product.

Our searches indicate no barrier for H addition to N_2H_3 to make initially excited $N_2H_4{}^*$. We estimate, similar to reaction R-2, a capture rate constant of $2.8 \cdot 10^{14} T^{1/6}$ cm^3 mol^{-1} s^{-1}. The potential energy diagram for N_2H_4 by Klippenstein et al. [13] indicates that the fastest reaction for $N_2H_4{}^*$, except for collisional stabilization at high pressures, is through a low-barrier, loose TS to NH_2 + NH_2 (R18). In agreement with this finding, the indirect determination by Li et al. [56] supports a very fast rate for this step, which appears to be the dominating product channel for N_2H_3 + H.

The results for N_2H_3 + H are consistent with the results of Dievart and Catoire [46], who also report H_2NN to be the major product among the diazene isomers. They find that isodiazene is also favored with NH_2 as the abstracter, whereas the formation of trans-diazene is the preferred path when reacting with CH_3. Dievart and Catoire conclude that regardless of the co-reactant, the formation

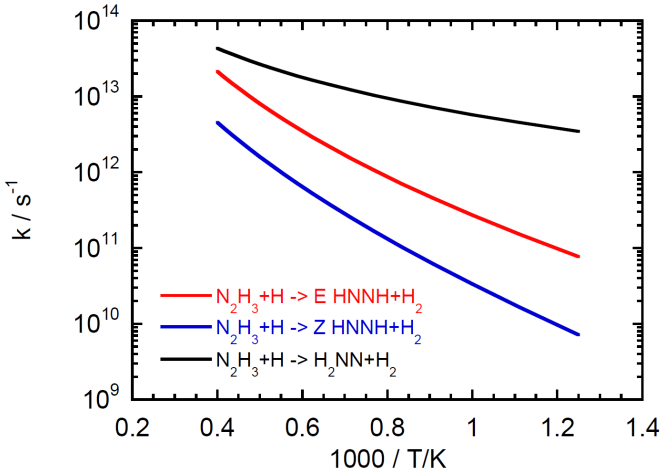

Figure 4: Arrhenius plot for the N_2H_3 + H reaction, based on the rate constants calculated in the present work.

of Z HNNH from N_2H_3 from these H-abstraction reactions is very unlikely since the associated saddle points lie about 12 to 38 kJ mol^{-1} above those for E HNNH [46].

The relative yields of the E and Z isomers of HNNH are of little consequence if they rapidly equilibrate at relevant temperatures. Figure 5 shows an Arrhenius plot for isomerization and dissociation of HNNH at atmospheric pressure, based on the rate constants calculated in the present work. Isomerization is faster than dissociation, implying that at high temperature the cis and trans isomers can be expected to attain partial equilibrium. However, due to the high activation energy, isomerization is hampered at lower temperatures.

Isomerization of Z HNNH to E HNNH via H-atom exchange,

$$\mathrm{H + Z\ HNNH \rightarrow N_2H_3^* \rightarrow H + E\ HNNH} \qquad \text{(R8)}$$

is an alternative pathway to equilibration. Other radicals than atomic hydrogen may also facilitate isomerization. The present calculations support the earlier

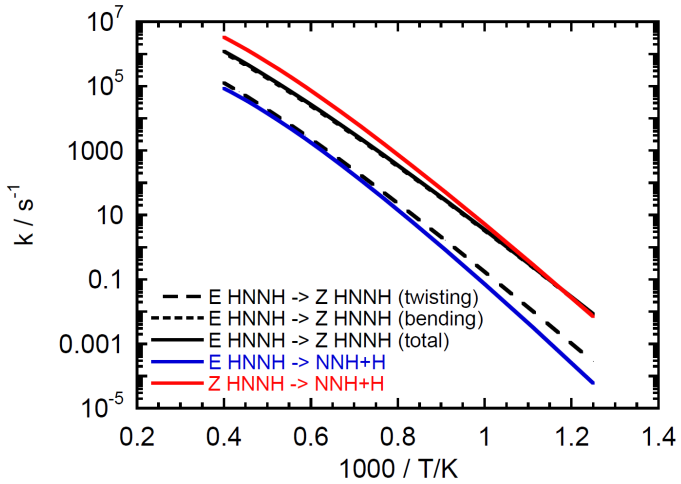

Figure 5: Arrhenius plot for isomerization and dissociation of HNNH at atmospheric pressure, based on the rate constants calculated in the present work.

conclusion [58] that for the trans isomer H-abstraction (R7) is faster than addition at the high-pressure limit, and extends this observation to the cis isomer too.

According to the present work, as well as the calculations of Dievart and Catoire [46] and Dean and Bozzelli [31], H-abstraction from N_2H_3 will form significant amounts of isodiazene. Dean and Bozzelli estimated rate constants for reactions of H_2NN with selected radicals, but other than their work, little is known about these steps. Based on the PES diagram in Fig. 2, the H + H_2NN reaction has several exothermic product channels, including H-abstraction

$$H + H_2NN \rightarrow H_2 + NNH$$

and H-assisted isomerization to HNNH. The barrier for H-abstraction was found to be small with density functional theory, and became slightly negative with CBS-APNO. There is likely an activation energy close to zero for this process. Due to the weak H-bond, possibly all H-abstraction reactions are comparatively fast.

To our knowledge, there are no data for diazene pyrolysis reported in the literature and it has not been possible to validate the subset established in the present work. It is of interest to investigate how the novel results for the diazene chemistry affect the kinetic modeling of ammonia and hydrazine pyrolysis and oxidation. However, there are ambiguities in the hydrazine formation and decomposition chemistry [60] that need to be addressed prior to such a study.

Conclusions

Quantum chemistry methods and unimolecular rate theory have been applied to characterize the pressure and temperature dependence of key reactions involved in diazene formation and consumption. Particular emphasis was put on the isomerization between the E (trans) and Z (cis) forms of HNNH and the relative importance of the diazene isomers. Rate constants are provided for isomerization and dissociation pathways for HNNH, addition of H atoms to form N_2H_3, abstraction by H atoms yielding short-lived NNH, and abstraction reactions of H with N_2H_3. These results, along with thermochemistry for the relevant isomers, are helpful to improve models of diamine chemistry, relevant to the combustion of NH_3 and N_2H_4. Results indicate that amine radical recombination mainly yields the E HNNH isomer, while H-abstraction from N_2H_3 results in E HNNH and H_2NN. However, at elevated temperature E $\rightarrow$ Z isomerization becomes competitive, and Z HNNH, being more reactive, acts to enhance the diazene consumption rate.

Acknowledgments

PM thanks the U.S. Department of Energy, Office of Basic Energy Sciences, Division of Chemical Sciences, Geosciences and Biosciences/Gas Phase Chemical Physics under Contract No. DESC0020952. Computational facilities were

provided by the National Science Foundation, Grant CHE-1531468. PG would like to acknowledge funding from Innovation Fund Denmark for the AEngine Grand Solutions project.

References

[1] P. Glarborg, A.D. Jensen, and J.E. Johnsson. Fuel nitrogen conversion in solid fuel fired systems. *Prog. Energy Combust. Sci.*, 29:89–113, 2003.

[2] P. Glarborg, J.A. Miller, B. Ruscic, and S.J. Klippenstein. Modeling Nitrogen Chemistry in Combustion. *Prog. Energy Combust. Sci.*, 67:31–68, 2018.

[3] A. Hayakawa, T. Goto, R. Mimoto, Y. Arakawa, T. Kudo, and H. Kobayashi. Laminar burning velocity and Markstein length of ammonia/air premixed flames at various pressures. *Fuel*, 159:98–106, 2015.

[4] A. Valera-Medina, H. Xiao, M. Owen-Jones, W. I. F. David, and P. J. Bowen. Ammonia for power. *Prog. Energy Combust. Sci.*, 69:63–102, 2018.

[5] H. Kobayashi, A. Hayakawa, K. K. A. Somarathne, and E. C. Okafor. Science and technology of ammonia combustion. *Proc. Combust. Inst.*, 37:109–133, 2019.

[6] A. Valera-Medina, F. Amer-Hatem, A.K. Azad, I. Dedoussi, M. De Joannon, R.X. Fernandes, P. Glarborg, H. Hashemi, X. He, S. Mashurk, J. McGowan, C. Mounaim-Rouselle, A. Ortiz-Prado, J.A. Ortiz-Valera, I. Rossetti, B. Shu, M. Yehia, H. Xiao, and M. Costa. A review on ammonia as a potential fuel: from synthesis to economics. *Energy Fuels*, 00:00–00, 2021.

[7] B. Mei, X. Zhang, S. Ma, M. Cui, H. Guo, Z. Cao, and Y. Li. Experimental and kinetic modeling investigation on the laminar flame propagation of ammonia under oxygen enrichment and elevated pressure conditions. *Combust. Flame*, 210:236–246, 2019.

[8] B. Mei, S. Ma, Y. Zhang, X. Zhang, W. Li, and Y. Li. Exploration on laminar flame propagation of ammonia and syngas mixtures up to 10 atm. *Combust. Flame*, 220:368–377, 2020.

[9] X. Han, Z. Wang, Y. He, Y. Zhu, and K. Cen. Experimental and kinetic modeling study of laminar burning velocities of NH_3/syngas/air premixed flames. *Combust. Flame*, 213:1–13, 2020.

[10] A. A. Konnov and J. De Ruyck. Kinetic modeling of the decomposition and flames of hydrazine. *Combust. Flame*, 124:106–126, 2001.

[11] H. Nakamura, S. Hasegawa, and T. Tezuka. Kinetic modeling of ammonia/air weak flames in a micro flow reactor with a controlled temperature profile. *Combust. Flame*, 185:16–27, 2017.

[12] D.-Y. Hwang and A. M. Mebel. Reaction mechanism of N_2/H_2 conversion to NH_3: a theoretical study. *J. Phys. Chem. A*, 107:2865–2874, 2003.

[13] S. J. Klippenstein, L. B. Harding, B. Ruscic, R. Sivaramakrishnan, N. K. Srinivasan, M.-C. Su, and J. V. Michael. Thermal decomposition of NH_2OH and subsequent reactions: Ab initio transition state theory and reflected shock tube experiments. *J. Phys. Chem. A*, 113:10241–10259, 2009.

[14] R. Asatryan, J. W. Bozzelli, G. da Silva, S. Swinnen, and M. T. Nguyen. Formation and decomposition of chemically activated and stabilized hydrazine. *J. Phys. Chem. A*, 114:6235–6249, 2010.

[15] P. Glarborg, H. Hashemi, S. Cheskis, and A.W. Jasper. On the Rate Constant for NH_2+HO_2 and Third Body Collision Efficiencies for NH_2+H(+M) and NH_2+NH_2(+M). *J. Phys. Chem. A*, 125:1505–1516, 2021.

[16] N. C. Baird and J. R. Swenson. Quantum Organic Photochemistry. IV. The Photoisomerization of Diimide and Azoalkanes. *Can. J. Chem.*, 51:3097–3101, 1973.

[17] N. W. Winter and R. M. Pitzer. Theoretical description of the diimide molecule. *J. Chem. Phys.*, 62:1269–1275, 1975.

[18] R. Ahlrichs and V. Staemmler. An ab initio study of the electronic structure of diimide. *Chem. Phys. Lett.*, 37:77–81, 1976.

[19] C. A. Parsons and C. E. Dykstra. Electron correlation and basis set effects in unimolecular reactions. A study of the model rearrangement system N_2H_2. *J. Chem. Phys.*, 71:3025–3033, 1979.

[20] C. J. Casewit and W. A. Goddard III. Thermochemistry of trans-diimide and 1,1-diazene. Ab initio studies. *J. Am. Chem. Soc.*, 102:4057–4062, 1980.

[21] H. J. A. Jensen, P. Joergensen, and T. Helgaker. Ground-state potential energy surface of diazene. *J. Am. Chem. Soc.*, 109:2895–2901, 1987.

[22] K. Kim, I. Shavitt, and J. E. Del Bene. Theoretical study of the di-imide (N_2H_2) molecule in ground and n $\rightarrow \pi^*$ excited states. *J. Chem. Phys.*, 96:7573–7579, 1992.

[23] N. Goldberg, M. C. Holthausen, J. Hrušák, W. Koch, and H. Schwarz. Mass-Spectrometric and GAUSSIAN2 Studies of the Diazene (HNNH) and Isodiazene (H_2NN) Molecules and Their Radical Cations. *Chem. Ber.*, 126:2753–2758, 1993.

[24] R. Cimiraglia and H.-J. Hofmann. Rotation and inversion states in thermal E/Z isomerization of aromatic azo compounds. *Chem. Phys. Lett.*, 217:430–435, 1994.

[25] C. Angeli, R. Cimiraglia, and H.-J. Hofmann. On the competition between the inversion and rotation mechanisms in the cis-trans thermal isomerization of diazene. *Chem. Phys. Lett.*, 259:276–282, 1996.

[26] B. S. Jursic. Ab initio and density functional theory study of the diazene isomerization. *Chem. Phys. Lett.*, 261:13–17, 1996.

[27] J. M. L. Martin and P. R. Taylor. Benchmark ab initio thermochemistry of the isomers of diimide, N_2H_2, using accurate computed structures and anharmonic force fields. *Mol. Phys.*, 96:681–692, 1999.

[28] M. Biczysko, L. A. Poveda, and A. J. C. Varandas. Accurate MRCI study of ground-state N_2H_2 potential energy surface. *Chem. Phys. Lett.*, 424:46–53, 2006.

[29] L. A. Poveda, M. Biczysko, and A. J. C. Varandas. Accurate ab initio based DMBE potential energy surface for the ground electronic state of N_2H_2. *J. Chem. Phys.*, 131:044309, 2009.

[30] A. Sindhu, R. Pradhan, U. Lourderaj, and M. Paranjothy. Theoretical investigation of the isomerization pathways of diazenes: torsion vs. inversion. *Phys. Chem. Chem. Phys.*, 21:15678–15685, 2019.

[31] A. M. Dean and J. W. Bozzelli. Combustion chemistry of nitrogen. In W.C. Gardiner, editor, *Gas phase combustion chemistry*, chapter 2. Springer-Verlag, 2000.

[32] Y. Zhao and D. G. Truhlar. The M06 suite of density functionals for main group thermochemistry, thermochemical kinetics, noncovalent interactions, excited states, and transition elements: two new functionals and systematic testing of four M06-class functionals and 12 other functionals. *Theoretical chemistry accounts*, 120:215–241, 2008.

[33] R. B. J. S. Krishnan, J. S. Binkley, R. Seeger, and J. A. Pople. Self-consistent molecular orbital methods. XX. A basis set for correlated wave functions. *J. Chem. Phys.*, 72:650–654, 1980.

[34] I. M. Alecu, J. Zheng, Y. Zhao, and D. G. Truhlar. Computational thermochemistry: scale factor databases and scale factors for vibrational frequencies obtained from electronic model chemistries. *J. Chem. Theory Comput.*, 6:2872–2887, 2010.

[35] J. W. Ochterski, G. A. Petersson, and J. A. Montgomery Jr. A complete basis set model chemistry. V. Extensions to six or more heavy atoms. *J. Chem. Phys.*, 104:2598–2619, 1996.

[36] M. J. Frisch, G.W. Trucks, H. B. Schlegel, G. E. Scuseria, M. A. Robb, J. R. Cheeseman, G. Scalmani, V. Barone, G. A. Petersson, H. Nakatsuji, X. Li, M. Caricato, A. V. Marenich, J. Bloino, B. G. Janesko, R. Gomperts, B. Mennucci, H. P. Hratchian, J. V. Ortiz, A. F. Izmaylov, J. L. Sonnenberg, Williams, F. Ding, F. Lipparini, F. Egidi, J. Goings, B. Peng, A. Petrone, T. Henderson, D. Ranasinghe, V. G. Zakrzewski, J. Gao, N. Rega, G. Zheng, W. Liang, M. Hada, M. Ehara, K. Toyota, R. Fukuda, J. Hasegawa, M. Ishida, T. Nakajima, Y. Honda, O. Kitao, H. Nakai, T. Vreven, K. Throssell, J. A. Montgomery Jr., J. E. Peralta, F. Ogliaro, M. J. Bearpark, J. J. Heyd, E. N. Brothers, K. N. Kudin, V. N. Staroverov, T. A. Keith, R. Kobayashi, J. Normand, K. Raghavachari, A. P. Rendell, J. C. Burant, S. S. Iyengar, J. Tomasi, M. Cossi, J. M. Millam, M. Klene, C. Adamo, R. Cammi, J. W. Ochterski, R. L. Martin, K. Morokuma, O. Farkas, J. B. Foresman, and D. J. Fox. Gaussian 16 rev. a03. *Wallington, CT, USA*, 2016.

[37] B. Ruscic and D.H. Bross. *Active Thermochemical Tables (ATcT), version 1.122p.* (available at ATcT.anl.gov), accessed April 2021.

[38] J. F. Stanton, J. Gauss, L. Cheng, M. E. Harding, D. A. Matthews, P. G. Szalay, A. A. Auer, R. J. Bartlett, U. Benedikt, C. Berger, D. E. Bernholdt, Y. J. Bomble, O. Christiansen, F. Engel, R. Faber, M. Heckert, O. Heun, C. Huber, T.-C. Jagau, D. Jonsson, J. Juselius, K. Klein, W. J. Lauderdale, F. Lipparini, T. Metzroth, L. A. MÃ$\frac{1}{4}$ck, D. P. O'Neill, D. R. Price, E. Prochnow, C. Puzzarini, K. Ruud, F. Schiffmann, W. Schwalbach, C. Simmons, S. Stopkowicz, A. Tajti, J. Vazquez, F. Wang, and J.D. Watts. *Cfour.* (available at http://www.cfour.de), 2019.

[39] S. J. Klippenstein, L. B. Harding, P. Glarborg, and J. A. Miller. The role of NNH in NO formation and control. *Combust. Flame*, 158:774–789, 2011.

[40] J. Troe. Predictive possibilities of unimolecular rate theory. *J. Phys. Chem.*, 83:114–126, 1979.

[41] J. Troe. Fall-off curves of unimolecular reactions. *Ber. Bunsenges. Phys. Chem.*, 78:478–488, 1974.

[42] J. Troe and V. G. Ushakov. Revisiting falloff curves of thermal unimolecular reactions. *J. Chem. Phys.*, 135:054304, 2011.

[43] C. J. Cobos and J. Troe. Prediction of reduced falloff curves for recombination reactions at low temperatures. *Z. Phys. Chem.*, 217:1031–1044, 2003.

[44] J. Troe. Theory of thermal unimolecular reactions in the fall-off range. I. Strong collision rate constants. *Ber. Bunsenges. Phys. Chem.*, 87:161–169, 1983.

[45] N. A. West, T. J. Millar, M. Van de Sande, E. Rutter, M. A. Blitz, L. Decin, and D. E. Heard. Measurements of Low Temperature Rate Coefficients for the Reaction of CH with CH_2O and Application to Dark Cloud and AGB Stellar Wind Models. *Astrophys. J.*, 885:134, 2019.

[46] P. Diévart and L. Catoire. Contributions of Experimental Data Obtained in Concentrated Mixtures to Kinetic Studies: Application to Monomethylhydrazine Pyrolysis. *J. Phys. Chem. A*, 124:6214–6236, 2020.

[47] M. Quack and J. Troe. Complex Formation in Reactive and Inelastic Scattering: Statistical Adiabatic Channel Model of Unimolecular Processes III. *Ber. Bunsenges. Phys. Chem.*, 79:170–183, 1975.

[48] T. J. Lee. Comparison of the T1 and D1 diagnostics for electronic structure theory: a new definition for the open-shell D1 diagnostic. *Chem. Phys. Lett.*, 372:362–367, 2003.

[49] B. Ruscic. *Active Thermochemical Tables (ATcT) values based on ver. 1.118g of the Thermochemical Network*. (available at ATcT.anl.gov), 2019.

[50] E. Goos, A. Burcat, and B. Ruscic. *Ideal gas thermochemical database with updates from Active Thermochemical Tables*. (<ftp://ftp. technion. ac. il/pub/supported/aetdd/thermodynamics> mirrored at <http://garfield. chem. elte. hu/burcat/burcat. html>, accessed 2021.

[51] O. Skreiberg, P. Kilpinen, and P. Glarborg. Ammonia chemistry under fuel-rich conditions in a flow reactor. *Combust Flame*, 136:501–518, 2004.

[52] Z. Tian, Y. Li, L. Zhang, P. Glarborg, and F. Qi. An experimental and kinetic modeling study of premixed $NH_3/CH_4/O_2/Ar$ flames at low pressure. *Combust. Flame*, 156:1413–1426, 2009.

[53] R.J. Kee, F. Rupley, and J.A. Miller. Sandia thermodynamic database. Technical report, Sandia National Laboratories, 1991.

[54] Y. Li and S. M. Sarathy. Probing hydrogen–nitrogen chemistry: A theoretical study of important reactions in NxHy, HCN and HNCO oxidation. *Int. J. Hydrogen Energy*, 45:23624–23637, 2020.

[55] D. P. Linder, X. Duan, and M. Page. Thermal rate constants for R + N_2H_2 → RH + NNH (R = H, OH, NH_2) determined from multireference configuration interaction and variational transition state theory calculations. *J. Chem. Phys.*, 104:6298–6307, 1996.

[56] S. Li, D. F. Davidson, and R. K. Hanson. Shock tube study of the pressure dependence of monomethylhydrazine pyrolysis. *Combust. Flame*, 161:16–22, 2014.

[57] Y.-Y. Chuang and D. G. Truhlar. Improved dual-level direct dynamics method for reaction rate calculations with inclusion of multidimensional tunneling effects and validation for the reaction of H with trans-N_2H_2. *J. Phys. Chem. A*, 101:3808–3814, 1997.

[58] J. Zheng, R. J. Rocha, M. Pelegrini, L. F. A. Ferrão, E. F. V. Carvalho, O. Roberto-Neto, F. B. C. Machado, and D. G. Truhlar. A product branching ratio controlled by vibrational adiabaticity and variational effects: Kinetics of the H + trans-N_2H_2 reactions. *J. Chem. Phys.*, 136:184310, 2012.

[59] M. Dontgen and K. Leonhard. Discussion of the separation of chemical and relaxational kinetics of chemically activated intermediates in master equation simulations. *J. Phys. Chem. A*, 121:1563–1570, 2017.

[60] L. Dai, S. Gersen, P. Glarborg, H. Levinsky, and A. Mokhov. Experimental and numerical analysis of the autoignition behavior of NH_3 and NH_3/H_2 mixtures at high pressure. *Combust. Flame*, 215:134–144, 2020.